Supporting Information

Anchored Ag^+ Sites on a Thiacalix[4]arene-Stabilized Ti–oxo Cluster Enable Efficient CO_2-to-CO Electroreduction

Qian Han,[a] Xiao Wei Wang,[b] Hong Yan Zhu,[b] Ru Xing Meng,[b] Lan Yan Li,[c] Wei-Dong Yu [c] and Chao Liu*[b]

[a] Xiangya School of Basic Medical Sciences, Central South University, Changsha 410083, Hunan, P. R. China.

[b] Xiangya School of Basic Medical Sciences, Central South University, Changsha 410083, Hunan, P. R. China

[c] School of Resources and Environment, Hunan University of Technology and Business, Changsha 410000, P. R. China

1. Experimental Section

Materials and Instruments All other reagents and solvents were purchased commercially and were not further purified when used. Powder X-ray difraction (PXRD) analysis were performed on a Rigaku Mini Flex II diffractometer at a 2θ range of 5–50° with Cu Kα radiation. Infrared spectra (KBr) were recorded on Nicolet 6700 spectrometer FT-IR spectrophotometer (Thermo Fisher Scientific, USA). Diffuse reflectance spectra were obtained on UV-4000 spectrophotometer. Electrospray ionization mass spectrometry (ESI-MS) experiments were performed on a Bruker Daltonik GmbH (Bruker, Germany). Photoelectrochemical tests were performed on a CHI 660E electrochemical workstation.

Single-Crystal X-ray Diffraction Analysis SCXRD analysis was conducted using a Rigaku XtalAB Synergy DS diffractometer equipped with graphite-monochromated Cu Kα radiation, operating at approximately 150 K. Absorption corrections were applied through SADABS software. The structural elucidation was carried out utilizing dual-space direct methods via ShelxT,[1] and subsequent refinements were performed employing the full-matrix least-squares method on F^2, facilitated by SHELXL-2014 software.[2,3] Non-hydrogen atoms were refined anisotropically to account for variations in electron density. The presence of rotational disorder in tert-butyl groups and extended alkane chains necessitated the application of ISOR, DELU, and SIMU constraints in all instances to ensure analytical convergence. Hydrogen atoms were modeled theoretically, positioned on their parent atoms, and their thermal parameters were kept fixed during refinement. In every cluster analyzed, some solvent molecules were markedly disordered, and as such, their corresponding hydrogen atoms were omitted from the refinement process. The SQUEEZE tool in PLATON software was utilized to handle severely disordered solvent molecules within the crystal structures. Multi-scan techniques were applied for all absorption corrections. The comprehensive crystallographic data derived from these analyses are compiled in Supplementary Table S1. CCDC 2493238, 2349620 contain the supplementary crystallographic data for this paper, which is available freely from the Cambridge Crystallography Data Centre.

Reference：

1. Sheldrick, G. M. SADABS: Program for Area Detector Adsorption Correction; University of Göttingen: Göttingen, Germany, 1996.
2. Sheldrick, G. M. SHELXL-2014/7: A Program for Structure Refinement; University of Göttingen: Göttingen, Germany, 2014.
3. Dolomanov, O. V.; Bourhis, L. J.; Gildea, R. J. J.; Howard, A. K.; Puschmann, H. OLEX^2: a complete structure solution, refinement and analysis program. J. Appl. Crystallogr. 2009, 42, 339−341.

Synthesis of Compounds

Synthesis for the cluster Ti_2-Sal: TC4A (23 mg, 0.032mmol), salicylic acid (14 mg, 0.1 mmol), and 3 mL of CH_3CN were combined in a 15 mL glass bottle. To this mixture, $Ti(O^iPr)_4$ (100 uL, 0.33 mmol) was added dropwise. The solution underwent sonication for 5 minutes and was subsequently placed in an oven at 80℃ for a period of 3 days. Yellow colored crystals were obtained after cooling to 25 °C in a yield of ~30% (based on TC[4]A).

Synthesis for Ti_6Ag_6: TC4A (36 mg, 0.05 mmol) and $AgCF_3SO_3$ (22 mg, 0.1 mmol) were added to 15 mL glass vials containing a mixed solvent of CH_3CN and DMF (4 mL, v/v = 3:1). Formic acid (10 μL, 0.265 mmol) and $Ti(O^iPr)_4$ (100 μL, 0.33 mmol) were then added dropwise. The mixture was sonicated for 15 minutes and subsequently incubated in an oven at 80°C for 3 days. Upon cooling to room temperature (25 °C), orange striped crystals were harvested with a yield of approximately 70%, based on the amount of TC4A used.

Electrochemical Measurements

All electrolytic CO_2 reduction experiments were conducted in a flow cell reactor utilizing a three-electrode setup, connected to a CHI760E electrochemical workstation operating under chronopotentiometric mode. This configuration was specifically chosen to allow for precise measurement of Coulombic charges. The electrolyte solution used was 1 M KOH, with an Ag/AgCl electrode (immersed in a saturated KCl solution), an anion exchange membrane and a platinum plate serving as the reference electrodes, Ion migration channel and counter electrodes, respectively. Additionally, gas-diffusion layer, modified with catalysts, acted as the working electrode. The preparation of the working electrode was given as follows: 10 mg electrocatalysts and 2 mg carbon nanotube were mixed grounded, then 1 mL 0.5 wt% Nafion solution mixed with ethanol was added into the mixture and treated by sonication to form uniform catalyst ink. After sonication for 1 h, the ink was dropped directly onto a carbon paper (1 cm × 1 cm) with a catalyst loading density of ~1 mg cm^{-2} and dried. The carbon paper was purchased from Gao Shi Rui Lian (Tianjin) Optoelectronic Technology Co., Ltd., with the original manufacturer being SGL in Germany. The carbon paper has a thickness of approximately 0.1 mm and is hydrophilic on both sides. To ensure a stable environment, high-purity CO_2 was introduced into the gas chamber at a consistent flow rate of 24 cm^3/min, controlled by a digital mass flow controller (Horiba). The gas-phase products were then quantitatively analyzed using a GC, Huaai 9560 Gas Chromatograph, employing argon as the carrier gas. The Faradaic efficiencies (FEs) of the various products were determined using a specific formula:

$$FE_a = \frac{\frac{v \times C_a}{A \times V_m} \times Z_a \times F}{j_{total}} \times 100\%$$

where FE represents the Faradaic Efficiency of product a, v denotes the CO_2 gas flow rate (L.s^{-1}), Ca is the volumetric fraction of product a as detected by gas chromatography, A refers to the geometric area of the electrode (cm^{-2}), Vm is the molar volume (22.4 L mol^{-1}), Za signifies the number of electrons transferred for the reduction to product a, F is the Faradaic Constant (C mol^{-1}), and $jtotal$ is the total current density (mA cm^{-2}). Cell resistances were meticulously assessed using electrochemical impedance spectroscopy at an open circuit, with an 85% ohmic resistance correction applied to account for i-R compensation. Furthermore, all potential measurements were adjusted to the reversible hydrogen electrode (RHE) scale, using the equation E (vs. RHE) = E (vs. Ag/AgCl) + 0.059 × pH + 0.198 (Ag/AgCl vs. RHE) to ensure accurate comparison.

The testing method for electrochemically active surface area (ECSA) is as follows:

The measurement of electrochemical active surface area (ECSA) was conducted in an H-cell under scan rates ranging from 10 to 120. The electrolyte solution of the h-cell was 0.5 M $KHCO_3$, with an Ag/AgCl electrode (immersed in a saturated KCl solution), a cation exchange membrane and a platinum plate serving as the reference electrodes, ion migration channel and counter electrodes, respectively. The calculation of ECSA was according to the formula, ECSA = RfS, in which S represents the real surface area of the smooth metal electrode, equivalent to the geometric area of work electrode. The roughness factor (Rf) was obtained from the formula, Rf = Cdl/Cs, in which double layer capacitance (C_{dl}) was equal to the slope of the double-layer charging current *versus* the scan rate slope. In this work, the C_{dl} was estimated by plotting the $\Delta J = (Ja - Jc)$ at −0.02 V (*vs.* RHE), where Ja and Jc was the anodic and cathodic current density, respectively. The linear slope was equivalent to twice of the C_{dl}. And the Cs (general specific capacitance of metal oxide) corresponded to the average double layer capacitance of a smooth oxide surface about 60 μF cm^{-2}.

The testing method for electrochemical impedance spectroscopy (EIS) was as follow:

The electrochemical impedance spectroscopy (EIS) measurements were perpormed in a frequency range from 10^6 to 0.1 Hz in a h-cell. The electrolyte solution of the h-cell was 0.5 M $KHCO_3$, with an Ag/AgCl electrode (immersed in a saturated KCl solution), a cation exchange membrane and a platinum plate serving as the reference electrodes, ion migration channel and counter electrodes, respectively.

Computational Methods.

All the spin-polarized Density Functional Theory (DFT) calculations were conducted using the Vienna Ab-initio Simulation Package (VASP version 5.4.4).[1, 2] The exchange-correlation functional was addressed using the Perdew-Burk-Ernzerhof (PBE) functional under the generalized gradient approximation (GGA).[3] Electron-ion interactions were modeled via the projector-augmented wave (PAW) method, employing a plane-wave basis set with a cutoff energy of 400 eV.[4] The nanoclusters were positioned within a cubic simulation box measuring 24 Å on each side and were subject to optimization procedures. The inclusion of van der Waals interactions between the adsorbate and the interface was facilitated by the empirical density functional dispersion correction (DFT-D3). Structural optimizations were carried out using a 1x1x1 Monkhorst-Pack k-point grid. Convergence thresholds were established at 10^{-4} eV for energy and 0.02 eV/Å for forces.

Reference：
1. G. Kresse and J. Furthmüller, *Phys. Rev. B*, **1996**, 54, 11169.
2. G. Kresse and J. Furthmüller, *Comput. Mater. Sci.*, **1996**, 6, 15-50.
3. J. P. Perdew, M. Ernzerhof and K. Burke, *J. Chem. Phys*., **1996**, 105, 9982-9985.
4. P. E. Blöchl, Phys. Rev. B, **1994**, 50, 17953.
5. S. Grimme, *J Comput Chem*, **2006**, 27, 1787-1799.

2. Structure of Compounds

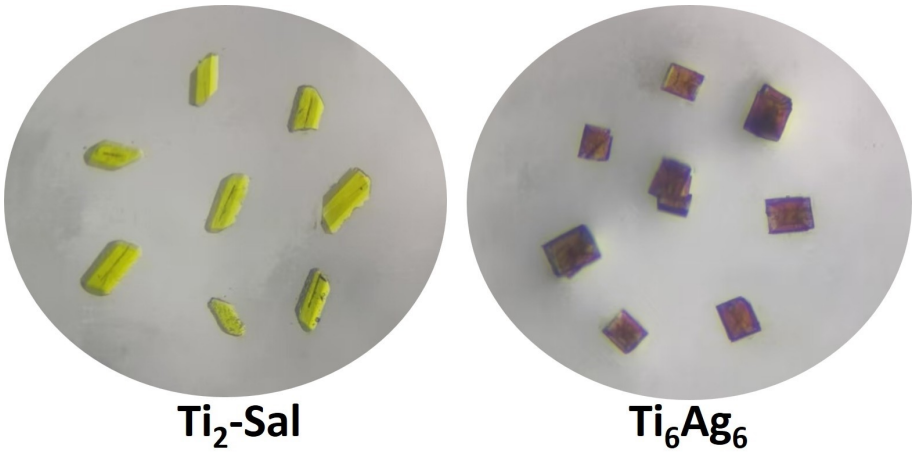

Figure S1. Pictures of fresh crystals of **Ti_2-Sal** and **Ti_6Ag_6**.

Table S1. X-ray measurements and structure solution of the compounds**.**

Compound CCDC	**Ti_2-Sal** 2493238	**Ti_6Ag_6** 2349620
Empirical formula	$C_{76}H_{104}N4O_{12}S_4Ti_2$	$C_{208}H_{258}Ag_6N_{16}O_{28}S_{16}Ti_6$
Formula weight	1489.67	4877.87
Temperature/K	150	150
Crystal system	monoclinic	triclinic
Space group	P21/n	P-1
a, Å	12.8614(5)	21.7650(3)
b, Å	13.3481(5)	21.8911(3)
c, Å	23.7581(9)	26.7368(2)
α/ °	90	70.5480(10)
β/°	91.259(3)	77.1850(10)
γ/°	90	87.9230(10)
V/Å^3	4077.7(3)	11702.9(3)
Z	2	2
ρ_{calcd}/gcm^{-3})	1.213	1.384
μ/mm^{-1})	0.356	7.422
F(000)	1584.0	5024.0
2Θ range for data collection/°	4.398 to 52	4.284 to 146.84
Reflections collected	7973	145575
Data/restraints/ parameters	7973/211/471	45342/712/23418
Goof	0.985	1.059
R_1/wR_2(I>2σ(I))	0.0915/ 0.2731	0.0441/0.1281
R_1/wR_2(all data)	0.1018/0.2852	0.0563/ 0.1360

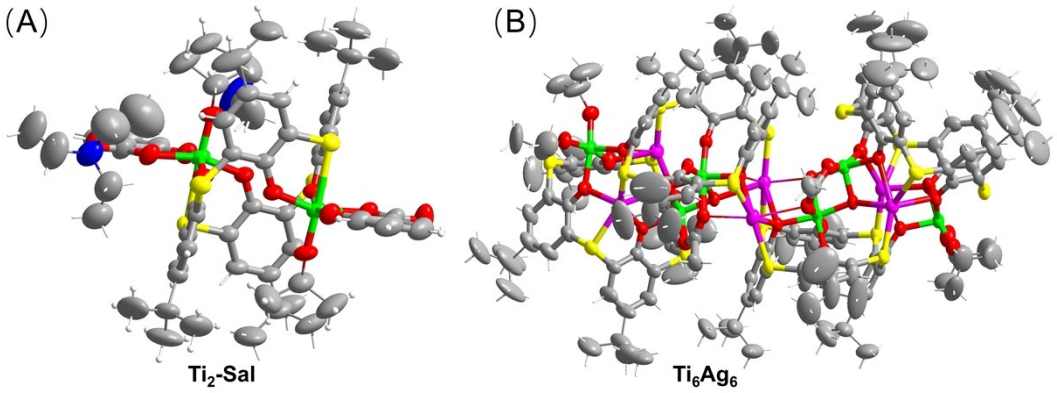

Figure S2. The molecular structures of the reported clusters in this article.

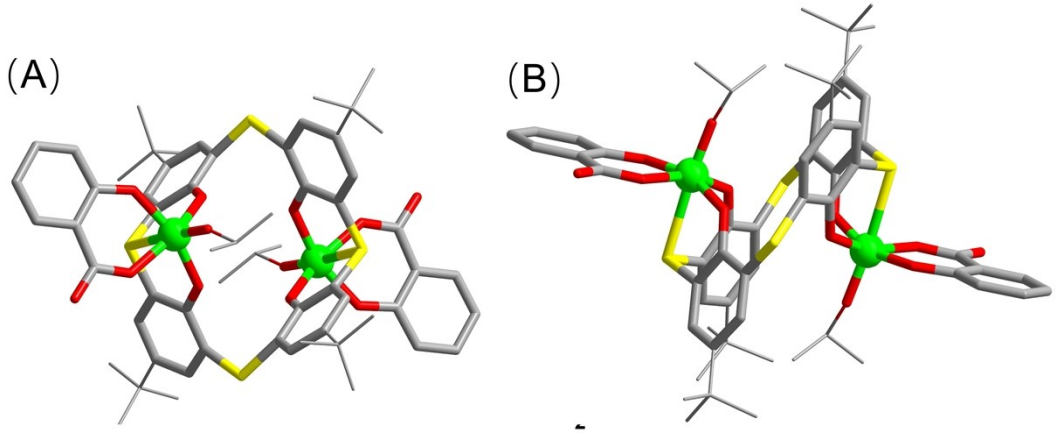

Figure S3. Illustration of the structure of **Ti_2-Sal**.

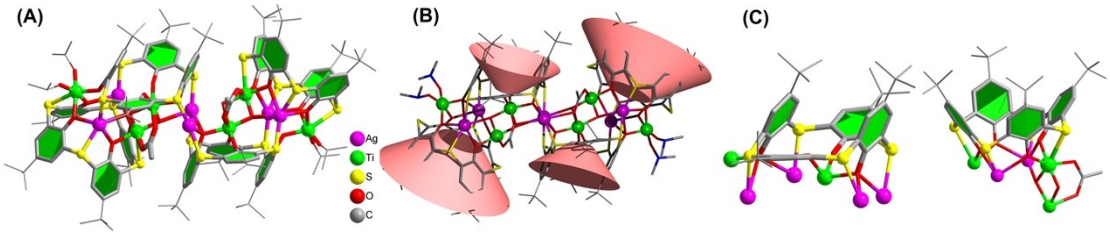

Figure S4. Illustration of the assembly of the **Ti_6Ag_6**.

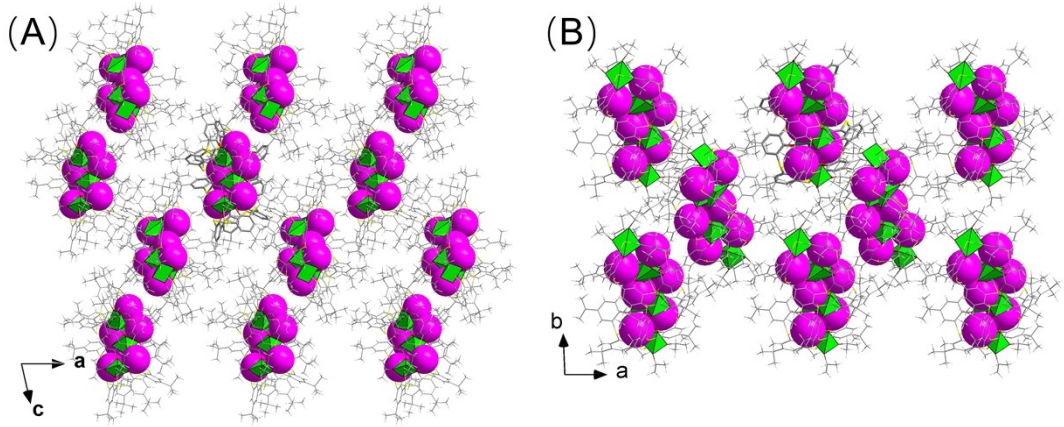

Figure S5. Three-dimensional packing structure of **Ti_6Ag_6** along the a and b axis.

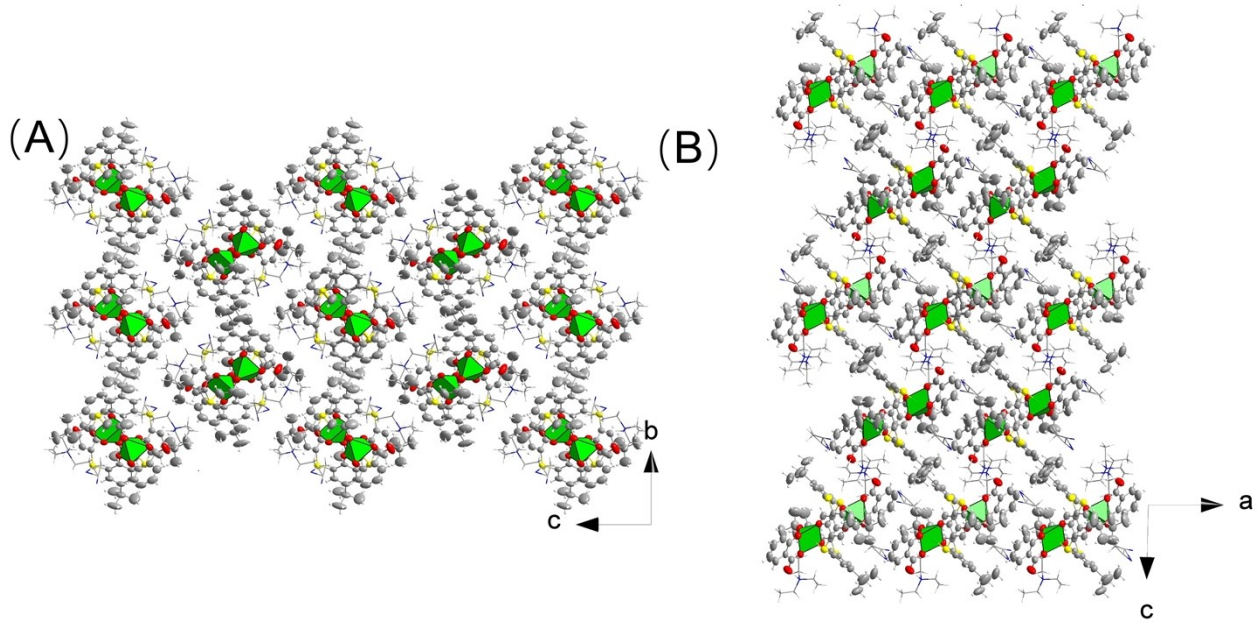

Figure S6. Three-dimensional packing structure of **Ti_2-Sal** along the a and b axis.

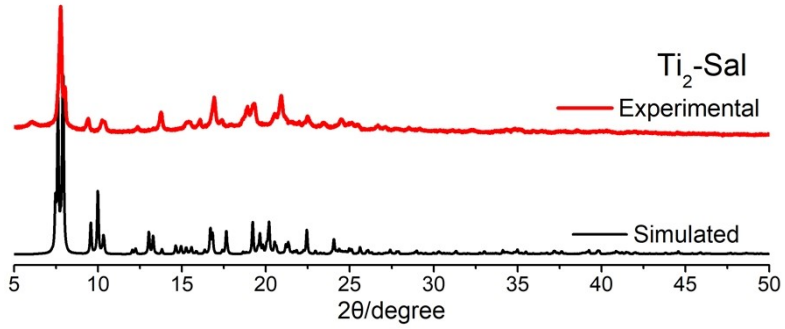

Figure S7. The XRD pattern of **Ti_2-Sal**.

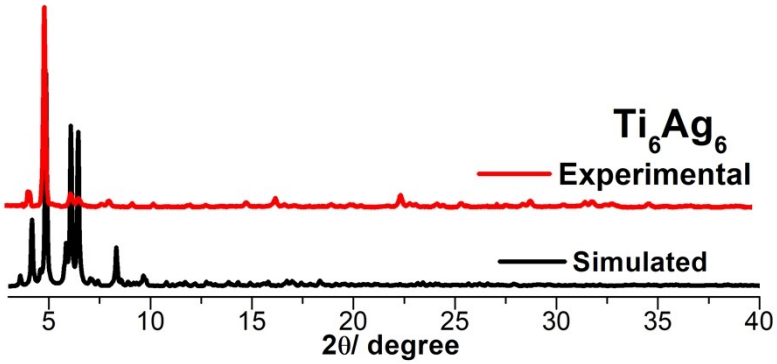

Figure S8. The XRD pattern of **Ti_6Ag_6**.

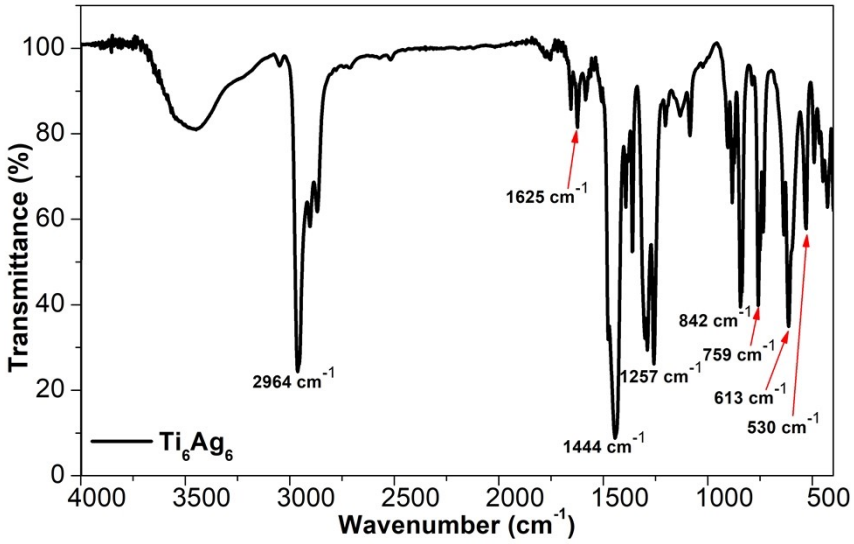

Figure S9. IR spectrum of crystal sample of **Ti_6Ag_6**.

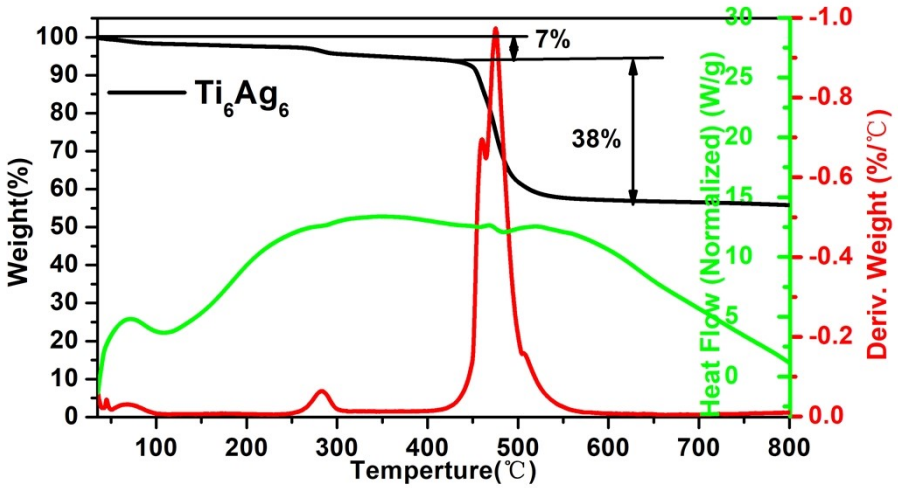

Figure S10. The TGA and DSC curves of **Ti_6Ag_6**.

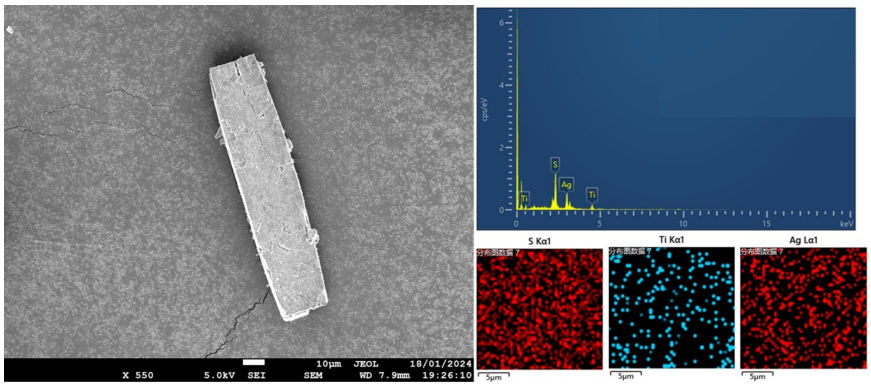

Figure S11. Morphology and elemental mapping of **Ti_6Ag_6**.

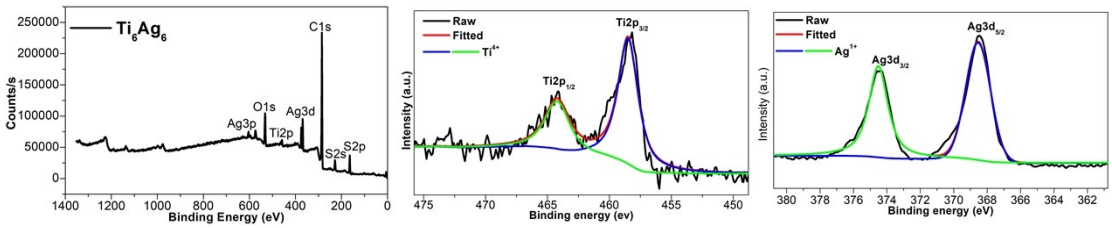

Figure S12. (A) XPS survey of **Ti_6Ag_6**. XPS survey of the **Ti_6Ag_6** showed the presence of Ti, Ag, S, C and O elements, consistent with the EDS mapping results; (B) High-resolution XPS spectra of Ti 2p in **Ti_6Ag_6**. The high-resolution Ti 2p spectrum shows two peaks at 458.48 and 464.19 eV that are assigned to the binding energy of Ti $2p^{3/2}$ and Ti $2p^{1/2}$ respectively; (C) High-resolution XPS spectra of Ag 3d in **Ti_6Ag_6**. The high-resolution Ag 3d spectrum shows two peaks at 368.29 and 374.39 eV that are assigned to the binding energy of Ag $3d^{5/2}$ and Ag $3d^{3/2}$ respectively.

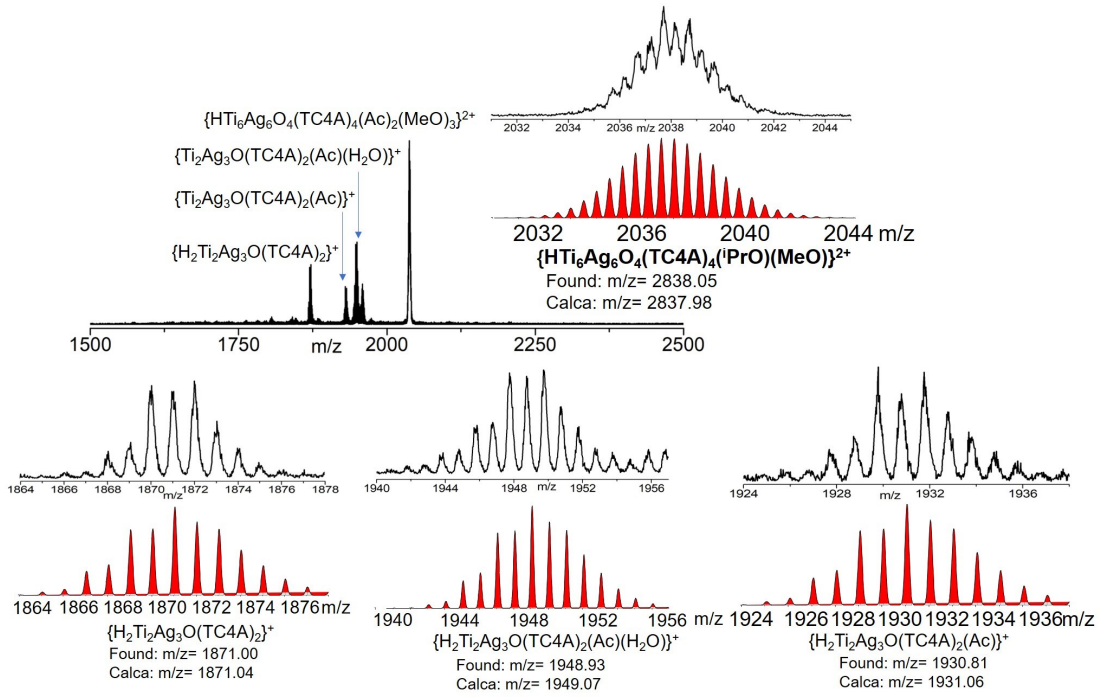

Figure S13. The positive ion ESI-MS of **Ti_6Ag_6** crystals in CH_2Cl_2/CH_3OH solution.

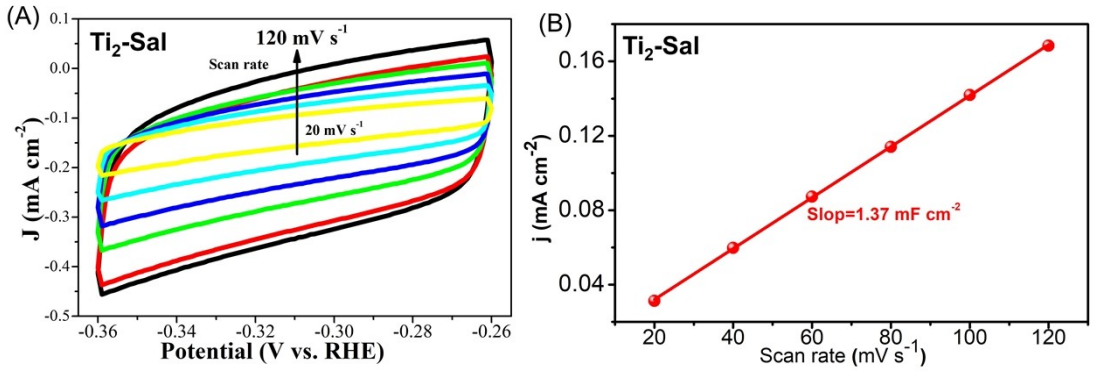

Figure S14. (A) The cyclic voltammograms (CVs) measurements with various scan rates for **Ti_2-Sal** in CO_2-saturated 0.5 M $KHCO_3$ electrolyte; (B) The capacitive current density ($J_a/2$-$J_c/2$) as a function of scan rate of **Ti_2-Sal**.

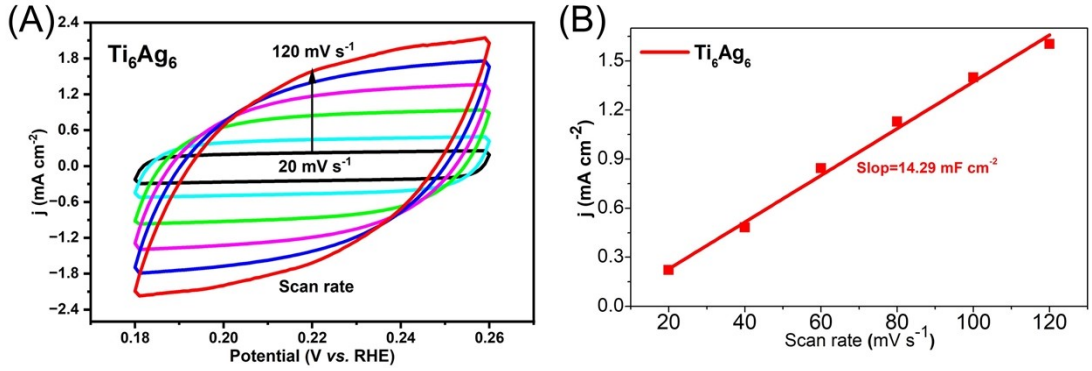

Figure S15. (A) The cyclic voltammograms (CVs) measurements with various scan rates for **Ti_6Ag_6** in CO_2-saturated 0.5 M $KHCO_3$ electrolyte; (B) The capacitive current density ($J_a/2$-$J_c/2$) as a function of scan rate of **Ti_6Ag_6**.

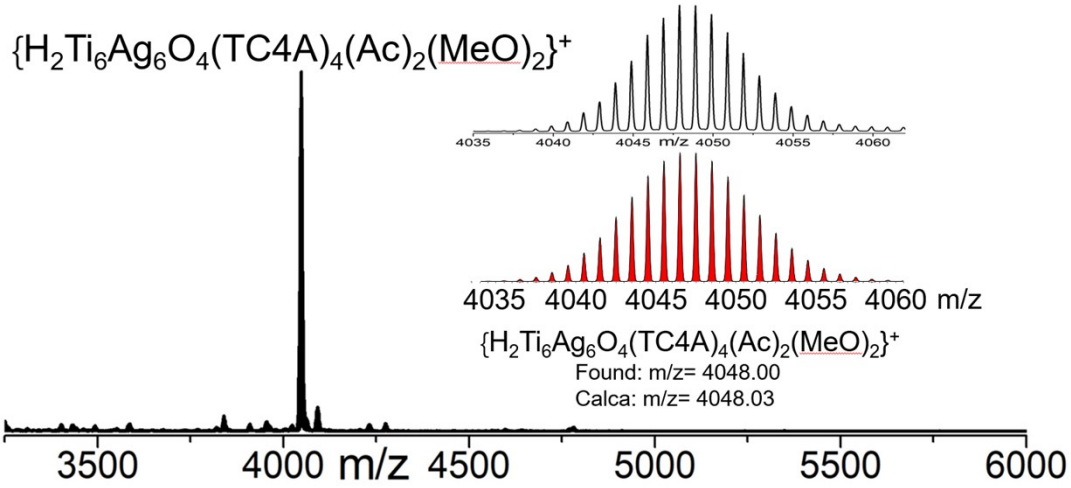

Figure S16. The positive ion ESI-MS of **Ti_6Ag_6** after electrocatalysis experiment.

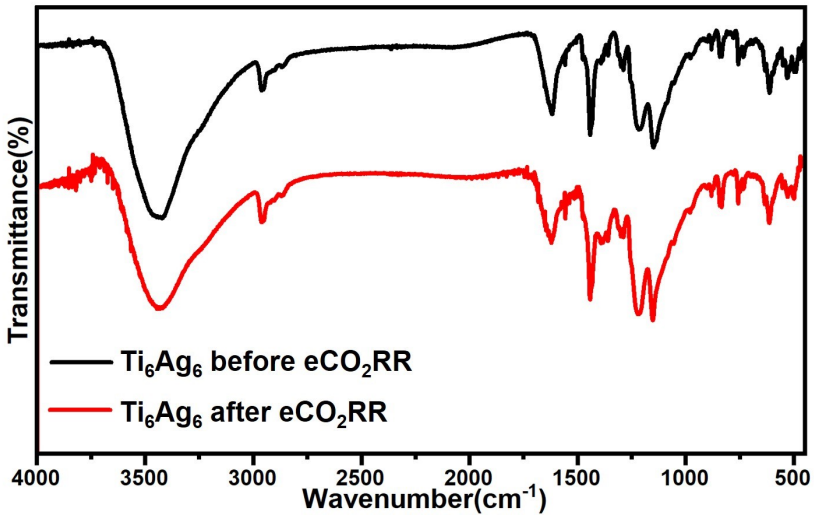

Figure S17. Comparison of the infrared spectra of the catalyst before and after the electrocatalytic reaction.

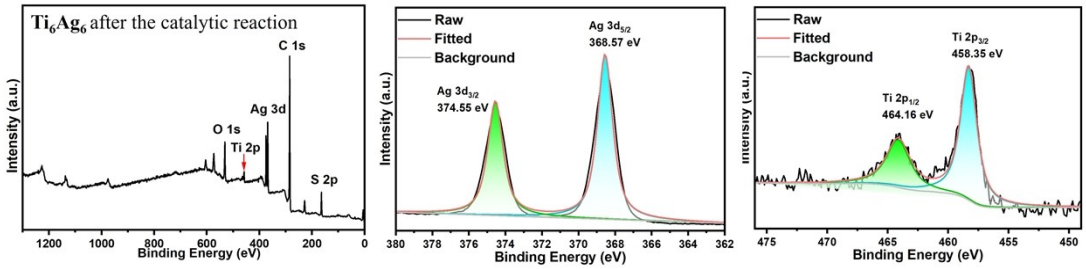

Figure S18. XPS spectra of the catalyst after the electrocatalytic reaction, indicating that the oxidation states of Ag and Ti remain unchanged.

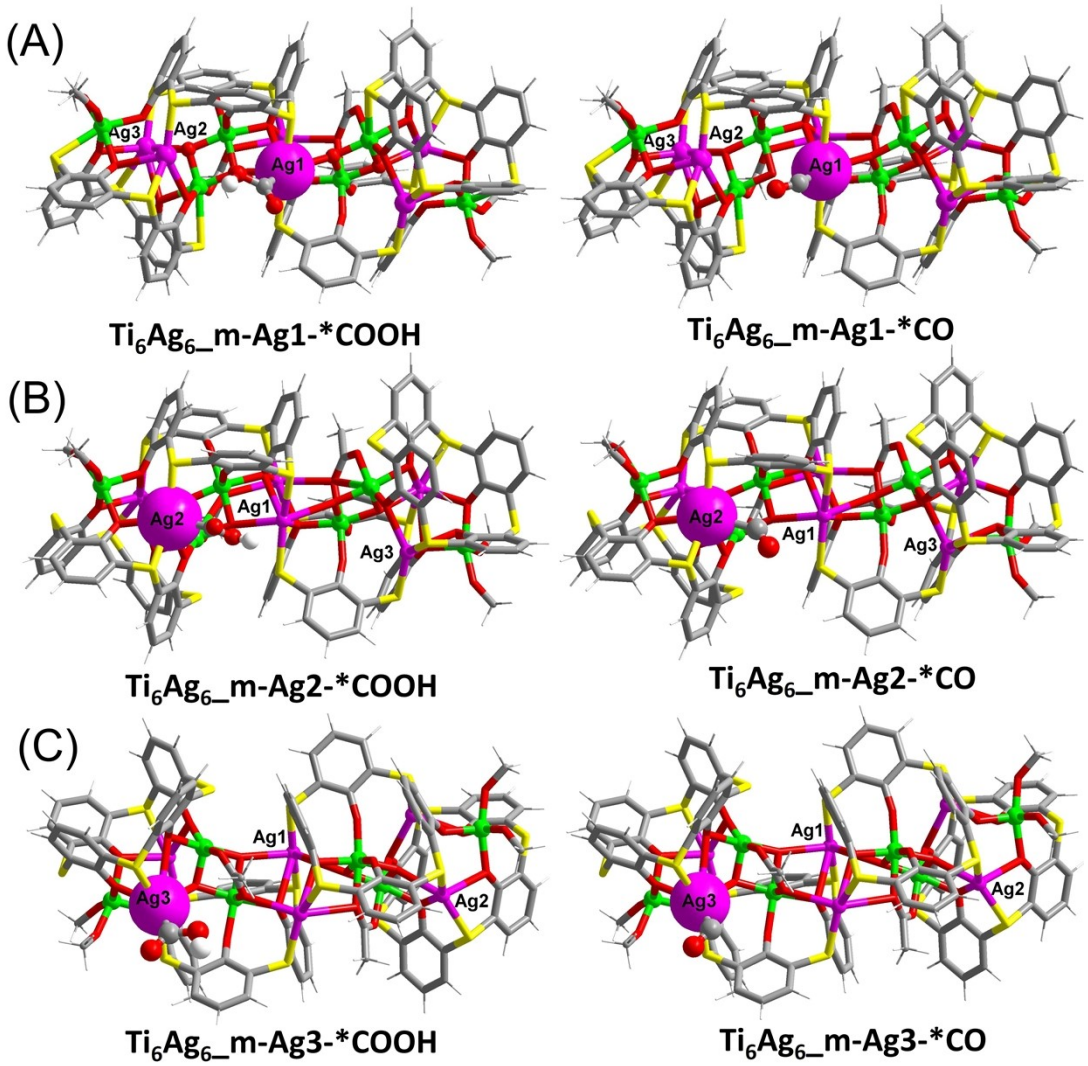

Figure S19. Optimized structures of the *COOH and *CO intermediates on the Ag(I) (A), Ag(II) (B),and Ag(III) (C) sites, respectively.

Table S2. Comparison of the electrocatalytic performances of Ag-based electrocatalysts for CO_2RR.

Catalyst	Application potential	Electrolyte	FE_{CO} (%)	Reference
Ti_6Ag_6	-1.0 V (vs. RHE)	1.0 M KOH	95.81	This work
Ti_8Ag_8	-0.9 V (vs. RHE)	1.0 M $KHCO_3$	92.4	S1
Ag_{30}	-0.9 V (vs. RHE)	1.0 M $KHCO_3$	93.4	S2
Zr_2Ag_7	-0.9 V (vs. RHE)	0.5 M $KHCO_3$	90.23	S3
Ag_{20}-Fc	-1.8 V (vs. RHE)	1.0 M KOH	98.68	S4
Ag-EPy-2	-0.7 V (vs. RHE)	0.1 M $KHCO_3$	74.0	S5
$Ag_{49}Mo_{16}$	-0.8 V (vs. RHE)	0.5 M $KHCO_3$	44.75	S6
Ag_{15}	-0.6 V (vs. RHE)	0.5 M $KHCO_3$	95.0	S7
Au_8Cu_1	-0.9 V (vs. RHE)	0.5 M K_2CO_3	~82.2%	S8
$Ag_{15}Cu_6$	-0.81 V (vs. RHE)	0.1 M $KHCO_3$	91.3	S9
Ag_9Cu_6	-0.89 V (vs. RHE)	0.1 M $KHCO_3$	48.5	S9
Ag_2Ti_{12}	-0.8 V (vs. RHE)	0.1 M $KHCO_3$	29.4	S10

The relevant references are as follows:

S1. Y-Q. Tian, W-L. Mu, L-L. Wu, X-Y. Yi, J. Yan, C. Liu, *Chem. Sci*, 2023, **14**, 10212-10218.

S2. L. J. Li, Y. T. Luo, Y. Q. Tian, P. Wang, X. Y. Yi, J. Yan, Y. Pei, C. Liu, *Inorg. Chem.*, 2023, **62**, 14377-14384.

S3. L. J. Li, W. L. Mu, Y. Q. Tian, W. D. Yu, L-Y. Li, J. Yan, C. Liu, *Chem. Sci*, 2024, **15**, 7643-7650.

S4. H-Y. Zhu, X-W. Wang, X-Y. Chen, L-Y. Li, Y-X. Li, W. D. Yu, J. Yan, C. Liu*, *Chem. Sci*, 2025, **16**, 20389-20396.

S5. M. Abdinejad, E. Irtem, A. Farzi, M. Sassenburg, S. Subramanian, H. P. I. van Montfort, D. Ripepi, M. R. Li, J. Middelkoop, A. Seifitokaldani, T. Burdyny, *ACS Catal.*, 2022, **12**, 7862-7876.

S6. S. Q. Li, L. F. Dai, Y. Q. Tian, X, Y, Yi, J. Yan, C. Liu, *Chem. Commun.*, 2023, **59**, 576-578.

S7. L. B. Qin, F. Sun, X. S. Ma, G. Y. Ma, Y. Tang, L. K. Wang, Q. Tang, R. C. Jin, Z. H. Tang, *Angew. Chem. Int. Ed.*, 2021, **60**, 26136-26141.

S8. S.Y Su, Y. T. Zhou, L. Xiong, S. Jin, Y. X. Du, M. Z. Zhu, *Angew. Chem. Int. Ed*. 2024, e202404629

S9. G. C. Deng, J. M. Kim, M. S. Bootharaju, F. Sun, K. Lee, Q. Tang, Y. J. Hwang, T. Hyeon, *J. Am. Chem. Soc.*, 2023, **145**, 3401-3407.

S10. Y. J. Liu, P. Shao, M. Y. Gao, W. H. Fang, J. Zhang, *Inorg. Chem.*, 2020, **59**, 11442-11448.